Deep-Sea Research II, Vol. 40, No. 6, pp. 1299–1326, 1993.
Printed in Great Britain.

0967–0645/93 $6.00 + 0.00

Baroclinic wind adjustment processes in the Mediterranean Sea

NADIA PINARDI* and ANTONIO NAVARRA*

(*Received* 15 *September* 1992; *in revised form* 2 *March* 1993; *accepted* 9 *June* 1993)

Abstract—The wind-driven general circulation of the Mediterranean Sea is studied using a primitive equation model. The model uses a 0.25° horizontal resolution and eight or 16 levels in the vertical. The model uses the Mediterranean basin geometry, and the Strait of Gibraltar is closed. The vertical density structure is initialized with annual average data, and the temperature and salinity values are fixed at the surface to simulate perpetual annual mean conditions. The wind forcing consists of monthly mean climatological stresses.

The results show that the general circulation of the Mediterranean Sea has a multiple time-scale character (seasonal excursions and steady state amplitudes are comparable) and it is composed by sub-basin scale gyres corresponding to the scale of the wind stress curl centers. The steady state circulation (annual mean average) is determined by a Sverdrup balance modified by viscous effects.

The unsteady vertically integrated transport circulation consists of sub-basin scale gyres similar to the steady state transport components, which amplify seasonally and the partial or total reversal of the currents in many subportions of the basin. The gyres can be stationary in position or propagating. This seasonal ocean response is partly constituted by Rossby modes due to the wind stress curl annual harmonic. The baroclinic circulation shows the seasonal shift of the North African Current from a position along the African coasts during winter to the center of the Balearic and Ionian basin during summer.

1. INTRODUCTION

THE Mediterranean Sea is one of the most extensively studied basins in the world. From the beginning of the century to very recent times, observations and studies have continued to accumulate, often without much coordination. Recently two international programs, POEM (Physical Oceanography of the Eastern Mediterranean, MALANOTTE-RIZZOLI and ROBINSON, 1989) and WMCE (Western Mediterranean Circulation Experiment, LA VIOLETTE, 1988) have started to collect new and reliable data sets to establish the mean circulation and its variability. Whereas a picture of the circulation starts to emerge from these data, the understanding of the general circulation and its physical and dynamical account is at its very beginning.

The Mediterranean basin is essentially formed by two large sub-basins, the Western (WM) and Eastern (EM) Mediterranean, separated by the shallow sill of the Strait of Sicily (~300 m deep) [Fig. 1(a)]. The WM can be subdivided into three regions, the Alboran Sea, the Balearic basin west and the Tyrrenhian Sea east of the Corsica–Sardinia islands. The EM contains two major sub-regional basins, the Adriatic and Aegean Sea, and it can be split into a western part, the Ionian Sea, and an eastern part, the Levantine basin,

*IMGA-CNR, Via Emilia Est 770, Modena, Italy.

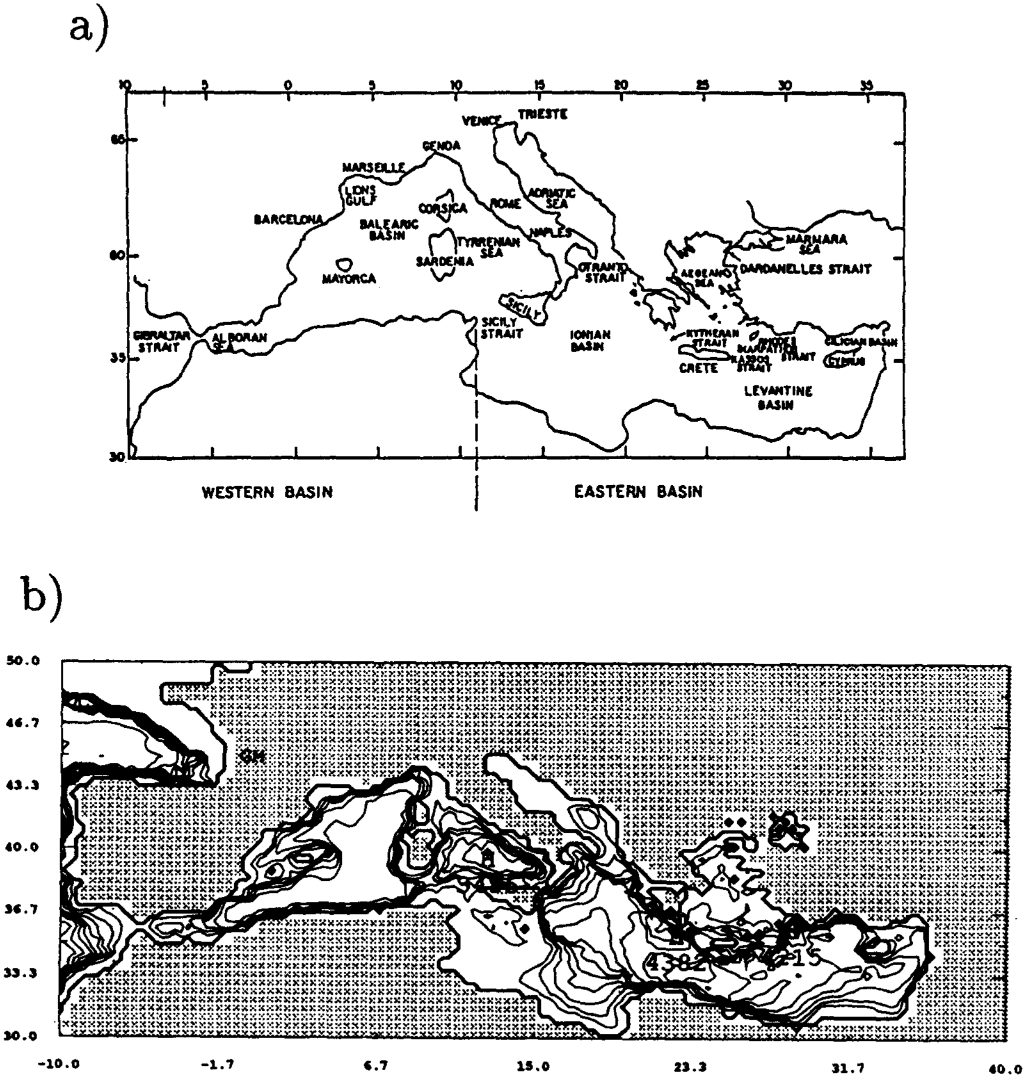

Fig. 1. (a) Basin nomenclature. (b) Mediterranean topography contours. Contour interval is 500 m.

separated by the island of Crete. We note the presence of eight major islands in the basin, Minorca, Majorca, Sardinia and Corsica in the WM, Sicily, Crete, Rhodes and Cyprus in the EM.

The whole Mediterranean basin extends ~30° in longitude and only ~10° in latitude; the WM southern border is 5° north of the corresponding EM southern border due to the large latitudinal excursion of the Tunisian coasts. The topographic relief is shown in Fig. 1(b). In the WM the topography consists of the large Balearic plane (~2500 m deep) and of the deep valley of the Tyrrhenian Sea ($\geq$ 3000 m). The EM topography shows a more complicated spatial structure than the WM relief. The Ionian basin reaches 3500 m with a

4000 m deep valley, the Hellenic basin, on its eastern side. The Levantine basin presents prominent seamounts and the 4000 m deep valley of the Rhodes basin, east of the island of Rhodes. The two sub-regional basins are shallower than 500 m in their northern part and in the south they reach a depth of ~1000 m. The continental rise is steep along part of the Maltese escarpment (east of the sill of Sicily), along the Egyptian coasts and all along the Hellenic arc.

The general circulation of the overall basin is driven by three main forcings: the inflow–outflow system at Gibraltar, the thermal and evaporative fluxes at the air–sea interface and the wind stress. The inflow–outflow at Gibraltar is the controlling mechanism for the salt and mass budget of the overall Mediterranean basin on the timescale of several decades (the water residence time in the Western Mediterranean is estimated to be of the order of 100 years). Low-salinity Atlantic water enters from Gibraltar at the surface and is transformed by intense air–sea interactions into deeper and saltier waters that finally exit into the Atlantic ocean. This complex water transformation process occurs seasonally in both the WM and EM basins. It is accomplished by large-scale thermal and evaporative fluxes, vertical turbulent mixing and regional deep water formation processes. The thermohaline forcing at the air–sea interface is important on the time-scale of seasons and the source–sink forcing due to deep water formation processes could play an important dynamical role on decadal time scales. The wind stress forces the circulation at seasonal time scales and at the spatial scale of major sub-portions of the Mediterranean basin. Thus it is possible that the thermal and wind forcing could be acting on the same time scales, the first inducing water transformation processes and the latter causing the transport and dispersal of such waters.

The classical observational picture of the baroclinic general circulation of the basin was first described by OVCHINNIKOV and FEDORSEYEV (1965) and LACOMBE (1975). Recently, extensive data campaigns in the framework of POEM and WMCE have revealed that the picture of the circulation is considerably richer. These studies have shown that the circulation of the Mediterranean is the result of a delicate interplay between mesoscale and seasonal variability (MILLOT, 1991; ROBINSON *et al.*, 1991).

In the WM, the circulation is composed of a cyclonic gyre in the Northern Balearic basin (also called the Liguro-Provençal gyre, CREPON *et al.*, 1989), a cyclonic gyre in the Tyrrhenian Sea, and a North African WM Current. The latter originates at the Strait of Gibraltar and it meanders up to the Strait of Sicily. An anticyclonic gyre in the southern Balearic basin (hereafter called the Algerian gyre) also can be present.

In the EM, the Ionian circulation is poorly known. However it is believed to consist of several anticyclonic and cyclonic gyres. There is also evidence that during the summer and in the southern Ionian an anticyclonic circulation is present. Its northern border is intensified by the EM North African Current entering from the Strait of Sicily. The Levantine basin offers a more complicated picture, with smaller gyres of opposite signs and a cyclonic gyre centered on the Rhodes basin (also called the Rhodes gyre, MILLIFF and ROBINSON, 1991). The southern part of the Levantine seems to be occupied by anticyclonic gyres called the Mersa-Matruh (ROBINSON *et al.*, 1991) and Shikmona gyres (ÖZSOY *et al.*, 1989).

In the recent past, the modelling efforts have concentrated on large sub-portions of the whole Mediterranean basin, generally the western and eastern basins. The effects of wind driving and realistic geometry–topography on the general circulation have been investigated. It should be mentioned that the first modelling results that showed an intense seasonal cycle in the EM were given by MENZIN and MOSKALENKO (1982). HEBURN (1987) studied with a reduced gravity model the wind-induced circulation in the WM. MALANOTTE-RIZZOLI and BERGAMASCO (1989, 1991) showed the general circulation in the EM with a linearized momentum primitive equation model by the wind, buoyancy and straits forcings. Results from these studies showed that the response to a time-dependent wind forcing is seasonally amplified. The only previous work that attempted a global Mediterranean wind driven study is by STANEV *et al.* (1989) but with very low horizontal resolution.

In this paper we present an idealized study of the wind adjustment processes in the Mediterranean basin geometry to try to clarify the dynamical nature of the response to winds. The models used in this study are based on the primitive equation model by BRYAN (1969) and COX (1984), with a vertical discretization chosen to describe accurately the low-order structure of the mean stratification (HECHT *et al.*, 1988). In practice results will be shown for eight and 16 vertical levels. These resolutions are probably still insufficient to fully resolve the bottom topography, but a full investigation of the bottom topography effects is beyond the scope of this paper that is centered on the ocean response to the winds in a Mediterranean-like situation.

2. THE MODEL AND THE DESIGN OF THE NUMERICAL EXPERIMENTS

We use the world ocean primitive equation general circulation model developed by BRYAN (1969) and COX (1984), adapted to the Mediterranean basin geometry. Here we synthetically write the equations and the parameterizations used while the numerical details can be found in the reference papers. The model equations are

$$\frac{\partial \vec{u}_h}{\partial t} + \vec{u} \cdot \nabla \vec{u}_h + \vec{f} \times \vec{u}_h = -\frac{1}{\rho_0}\vec{\nabla} p + A_h \nabla^2 \vec{u}_h + A_v \vec{u}_{hzz} \tag{1}$$

$$p_z = -\rho g \tag{2}$$

$$\nabla \cdot \vec{u} = 0 \tag{3}$$

$$\frac{\partial T}{\partial t} + \vec{u} \cdot \nabla T = K_h \nabla^2 T + Q_T^{CA} \tag{4}$$

$$\frac{\partial S}{\partial t} + \vec{u} \cdot \nabla S = K_h \nabla^2 S + Q_S^{CA} \tag{5}$$

$$\rho = \rho(T,S,p) \tag{6}$$

where the spherical coordinates (λ,θ,z) are considered, $\vec{u} = (u,v,w)$ is the velocity vector, $\vec{u}_h$ its horizontal components, $\vec{f} = 2\Omega\sin\theta\vec{k}$, p and ρ the pressure and density. T,S the temperature and salinity. The Boussinesq, hydrostatic approximations are made. The equation of state (6) is taken to be a nine-term, third-order polynomial approximation to the Knudsen formula for the density of seawater. A_h and K_h are constant turbulent diffusion coefficients and Q_T^{CA} and Q_S^{CA} represent the sources of heat and salinity due to the convective adjustment mixing parameterization in the model. The convective adjustment is introduced into the model assuming that at each grid point T,S properties are mixed between adjacent levels when gravitational instability (or $\rho_z > 0$) is established.

The boundary conditions considered are: at $z = 0$

$$A_v \vec{u}_{hz} = \vec{\tau} \tag{7}$$

$$T = T^* \tag{8}$$

$$S = S^* \tag{9}$$

$$w = 0 \tag{10}$$

where T^* and S^* are the climatological annual mean temperature and salinity fields of LEVITUS (1982). At $z = -H(x,y)$, where H is the topographic height, we impose:

$$w = -\vec{u}_h \cdot \nabla H \tag{11}$$

$$(T_z, S_z) = 0 \tag{12}$$

$$(u_z, v_z) = 0. \tag{13}$$

The boundary condition (7) is applied interpolating linearly between the HELLERMAN *et al.* (1983) monthly mean wind stresses, $\vec{\tau}$.

The coefficients of diffusion are chosen to be $A_h = 4.10^6\,\mathrm{cm^2\,s^{-1}}$, $A_v = 1.5\,\mathrm{cm^2\,s^{-1}}$, $K_h = 1.210^7\,\mathrm{cm^2\,s^{-1}}$, respectively. This choice gives an almost perfectly repeating cycle in the integrated kinetic energy of the basin.

The model has been set up at the horizontal resolution of 0.25° of latitude and longitude and with eight and 16 vertical levels. In Fig. 2 the model grid is shown for both resolutions. The coastline geometry is fairly well reproduced, but the northern Adriatic has been eliminated leaving only the middle and southern regions. The Strait of Gibraltar is considered to be closed so that no inflow–outflow processes are considered. The islands of Corsica–Sardinia and Minorca–Majorca have been connected as in the case of Sicily and the southern tip of the Italian peninsula. We left five isolated islands, Ibiza, Minorca–Majorca, Corsica–Sardinia, Crete and Cyprus; the island of Rhodes has been connected to the Turkish coast because of the low resolution of the model. The eight model levels are located at 30, 80, 120, 160, 230, 330, 490 and 110 m of depth and at 5, 15, 30, 50, 80, 120, 160, 200, 240, 280, 340, 420, 500, 1100, 2000, 3000 for the 16 levels case.

In Fig. 3 we show the wind stresses for four different months. The WM shows the Mistral wind stresses over the northern Balearic basin which persist throughout the seasons. The southern WM shows instead a reversal in the direction of the stresses between December–March and June–September conditions. In the EM the Summer stresses are meridional over the Ionian and Levantine basins and they become almost zonal in December. The annual mean curl of wind stress is composed by separate maxima and minima centers in each sub-basin; in the northern Balaeric basin we have a well known double gyre configuration [regions I–W and II–W in Fig. 3(e)] and a secondary center is present in the western Tyrrhenian (III–W). These curl centers will determine the annual mean circulation gyre systems if the response is linear. The time dependent response is going to be important where the annual variance is greater, e.g. in the southern Balearic (region IV–W) and in the Tyrrhenian (region V–W). In the EM we can see several curl centers all located south of the Hellenic arc (regions from I–E to IV–E) and almost zero average curl in the central Ionian basin. The Ionian is, in fact, a place of high annual curl variance as shown by the double maxima centers located in its Northern (V–E) and southern (VI–E) parts [Fig. 3(f)]. Finally, the Aegean Sea and northern Levantine basin display of absolute maxima in the curl variance as shown by region VII–E. In conclusion, the mean wind stress curl contains the vorticity centers which could sustain a mean multiple gyre circulation and its variance reaches relative maxima in separate sub-regions of the basin.

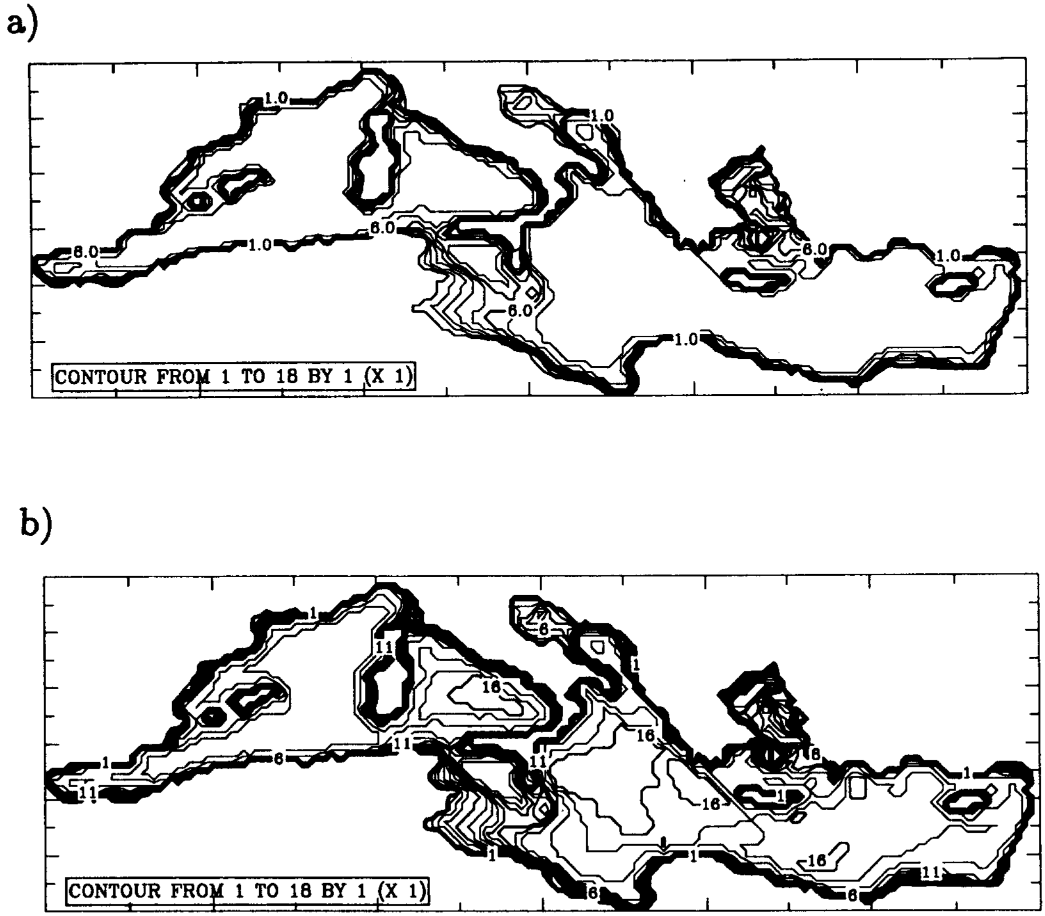

Fig. 2. (a) Model 0.25° discretized topography for the eight levels configuration. (b) Model discretized topography for the high resolution experiment with 16 levels.

To capture the principal components of the time dependent part of the wind stress curl and its spatial pattern, we did an harmonic analysis of the 12 months wind stress curl by writing

$$\hat{k} \cdot \nabla \times \vec{\tau} = \sum_{k=1}^{6} a_k(x,y) \cos\left(\omega_k t + \delta_k(x,y)\right) \tag{14}$$

where $\hat{k} \cdot \nabla\times$ is the vertical component of the curl operator (hereafter referred to as curl only), $\omega_k = 2\pi k/12$ is the frequency of the kth harmonic component, a_k its horizontal amplitude and δ_k the phase. The annual and semi-annual components are shown in Fig. 4. The annual harmonic amplitude captures all of the annual variance centers of Fig. 3(f) except in the region VI–E, which is shown to be important in the semi-annual harmonic amplitude. The annual harmonic amplitude is comparable to the annual average amplitude [Fig. 3(e)], the semi-annual component is the second largest while all the other

Table 1. Description of the experiments

Experiment name	Levels	Dynamical Configuration	Comments
C1	8	Monthly mean winds	Central experiment
C2	8	Annual mean wind, $\langle\vec{\tau}_{ij}\rangle$	Circulation induced by mean winds
C3	8	Wind anomalies $\vec{\tau}_{ij}' = \vec{\tau}_{ij} - \langle\vec{\tau}_{ij}\rangle$	Circulation induced by wind anomalies
C4	8	Monthly mean winds but $\beta = 0$	Beta experiment
C5	8	Monthly mean winds but homogeneous stratification	Homogeneous experiment
S1	8	$\vec{\tau}_{ij} = 0$ for $j \in [1, 38]$	Remote response of southern Balearic basin
S2	8	$\vec{\tau}_{ij} = 0$ for $i \in [1, 107]$	Response of the Ionian to remote wind forcing
S3	8	$\vec{\tau}_{ij} = 0$ for $i \in [107, 167]$	Response of the Ionian to local wind forcing
H1	16	Monthly mean winds	Central experiment high resolutions

components (not shown) are at smaller amplitude. The phase of the annual harmonic is generally small everywhere except at the Sicilian Strait, south of Crete and Cyprus. This means that the annual harmonic curl forcing is a perfectly repeating sinusoidal function at high amplitude but zero annual mean in the regions IV–W, V–W, V–E and VII–E, e.g. where the annual mean curl variance field had relative maxima centers. In conclusion, we expect that the time-dependent ocean circulation induced by climatological winds will be at seasonal time scales in the southern Balaeric, Tyrrhenian, Ionian and Aegean–northern Levantine basin.

The central numerical experiments (C1 and H1) consist of the monthly varying wind stresses, the temperature and salinity fields from annual mean climatological data and the two topographies mentioned above (Table 1). We change the wind forcing in experiments C2 and C3 to show the influence of the annual mean wind stress and of the wind anomalies, defined as the deviations from that mean. In experiment C4 we impose fictiously the Coriolis parameter as a constant, thus eliminating the effect of Rossby wave propagation, and experiment C5 has homogeneous stratification conditions. The rest of the experiments are sensitivity experiments to determine the local vs remote response of major subportions of the Mediterranean basin in the low vertical resolution case.

In Fig. 5 we show the basin integrated kinetic energy cycle for experiment C1 (the time series for H1 is very similar and is not shown here). We obtained an annually repeating cycle with two relative peaks, one during summer (September) and the largest during the winter season (March). The winter onset is the fastest growth of energy in the basin, the spring decay is slow, and the summer peak is approximately four times smaller than the winter one. The adjustment to a repeating cycle takes about 6 months due to the viscous adjustment of the baroclinic velocity field.

3. THE VERTICALLY INTEGRATED CIRCULATION

(a) The mean circulation

Here we describe the annual mean fields of transport streamfunction shown in Fig. 6 for the low vertical resolution experiments. We define as "barotropic" the vertically integrated momentum field and as "baroclinic" the departure from the vertical mean.

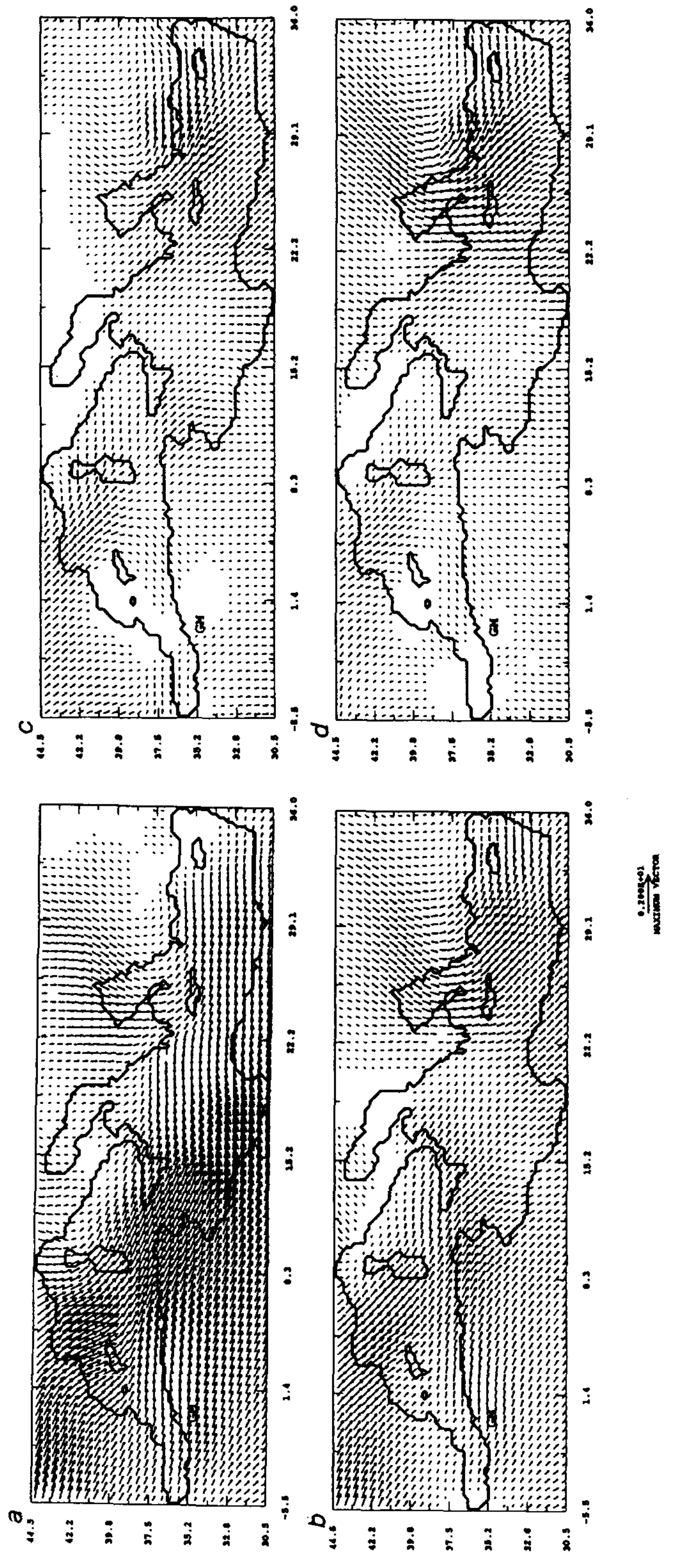
a
b
c
d

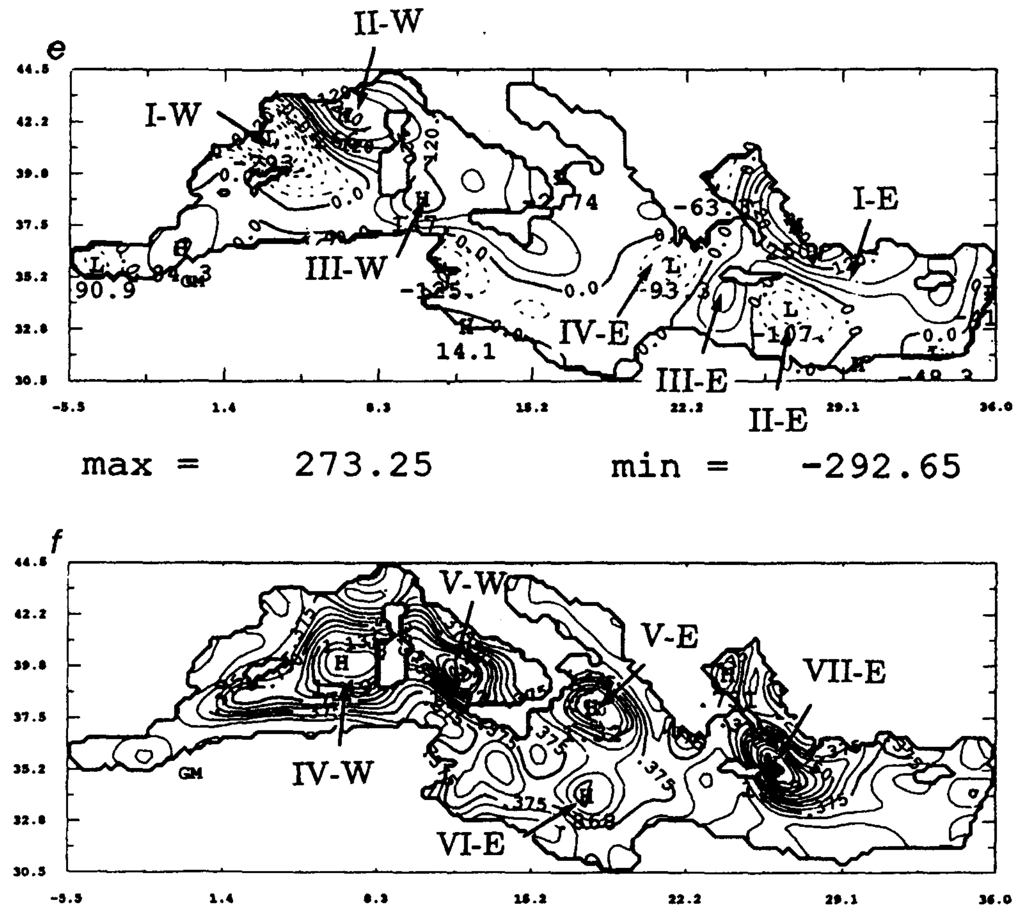

Fig. 3. (a) HELLERMANN and ROSENSTEIN (1983) wind stresses for four different months, e.g. (a) December, (b) March, (c) June, (d) September. The reference arrow on the right of the pictures is in units of dyne cm^{-2}. The white areas indicate wind stress magnitudes less than 0.01 dyne cm^{-2}. (e) Annual mean wind stress curl in units of 10^{-10} dyne cm^{-3} and the contour interval is 40×10^{-10} dyne cm^{-3}. (f) Variance of wind stress curl anomalies with respect to the annual mean.

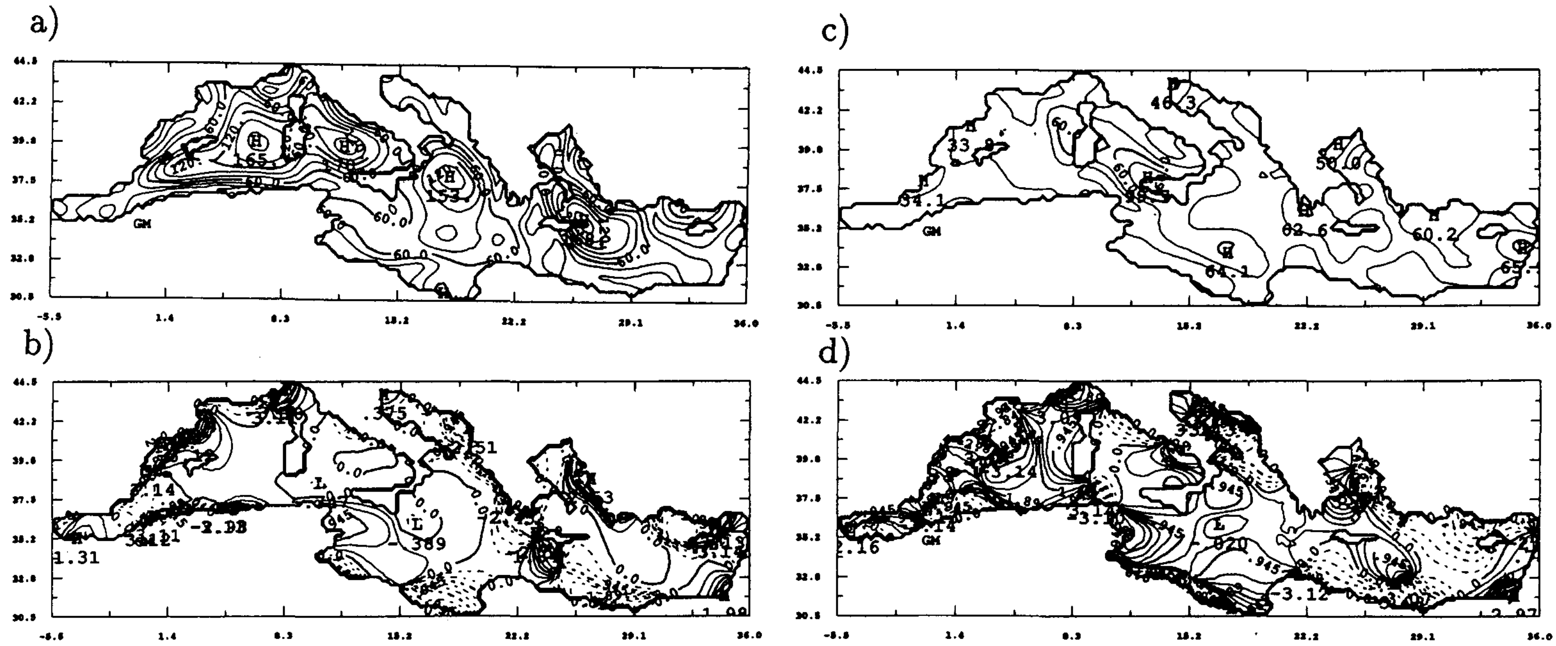

Fig. 4. Harmonic analysis of wind stress curl: (a) and (b) are the amplitude and the phase of the annual harmonic component respectively; (c) and (d) are the amplitude and phase of the semi-annual harmonic component. The contour interval is 20×10^{-10} dyne cm^{-3} for the amplitude and 0.1 radians for the phase fields.

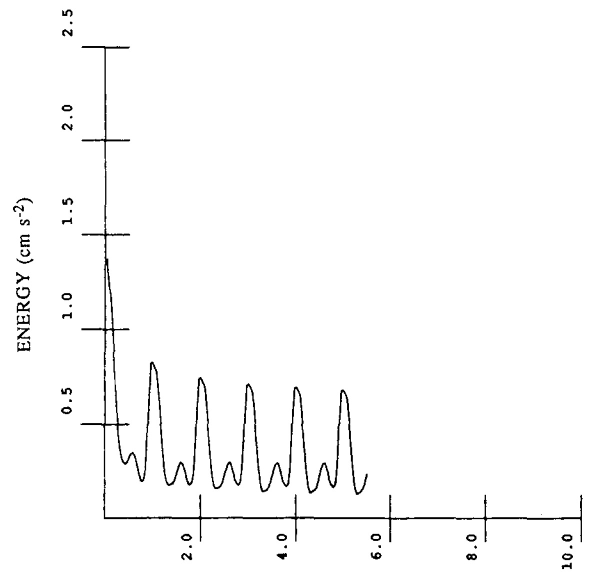

Fig. 5. Basin averaged kinetic energy for experiment C1 as a function of time.

The western basin mean circulation consists of the Liguro-Provençal cyclonic gyre and a cyclonic Tyrrhenian gyre, corresponding to the wind stress curl centers II–W and III–W of Fig. 3. On the eastern flank of the Minorca–Majorca island a weak anticyclonic circulation is also present, corresponding to the wind stress curl center I–W. The eastern basin shows four gyre centers: a cyclonic Rhodes gyre (corresponding to the curl center I–E), a Cretean dipole formed by an anticyclone south-east and a cyclone south-west of Crete (corresponding to the curl centers II–E and III–E), and a zonally elongated Ionian basin anticyclonic circulation. These gyres are consistently shifted westward with respect to their corresponding curl centers. The transport is weaker in the eastern basin gyres (~1 Sv in the Rhodes gyre) than in their western counterpart (~2 Sv in the Liguro-Provençal gyre).

The results (Fig. 6) can be understood by analyzing the vertically integrated vorticity equation of the model. In our formulation the vertically integrated transport streamfunction, ψ, is defined by

$$\bar{\vec{u}} = \frac{\hat{k} \times \nabla\psi}{H} = \frac{1}{aH}\left(\frac{\partial\psi}{\partial u}, m\frac{\partial\psi}{\partial\lambda}\right)$$

where $\bar{\vec{u}}$ is the vertically averaged velocity field, e.g.

$$\bar{\vec{u}} = \frac{1}{H}\int_{-H}^{0} \vec{u}\,\mathrm{d}z \tag{15}$$

and the total velocity field is $\vec{u} = \bar{\vec{u}} + \hat{\vec{u}}$ where $\hat{\vec{u}}$ is the depth dependent or baroclinic part of the velocity field. Furthermore, $\hat{k}$ is the unit vector pointing in the vertical direction, a is the earth's radius and $m = \sec\theta$. The equation for the vertically integrated vorticity field, ζ, defined as

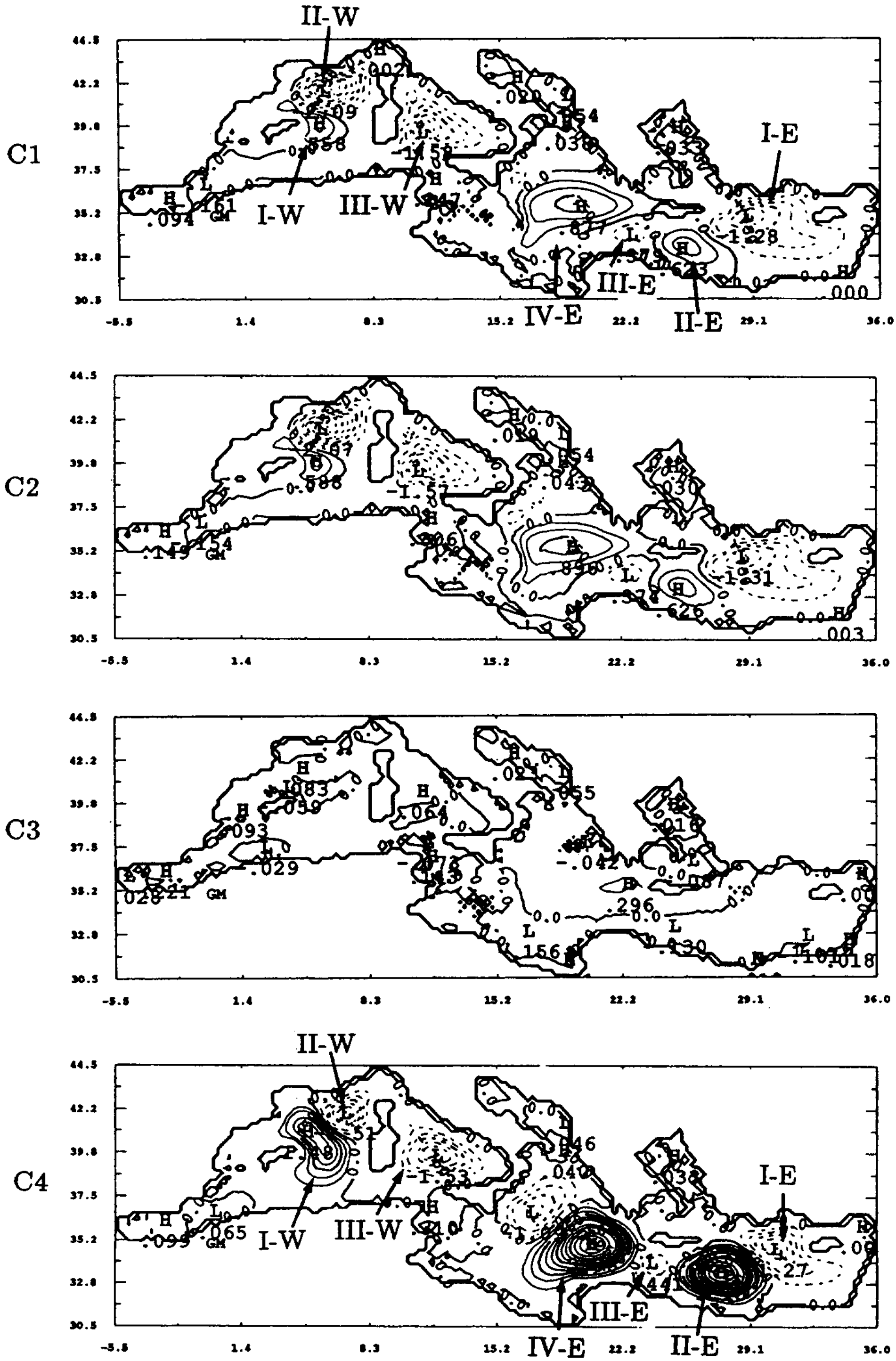
C1
C2
C3
C4
II-W
I-W
III-W
I-E
II-E
III-E
IV-E
44.5
42.2
39.8
37.5
35.2
32.8
30.5
-5.5
1.4
8.3
15.2
22.2
29.1
36.0

S1

S2

S3

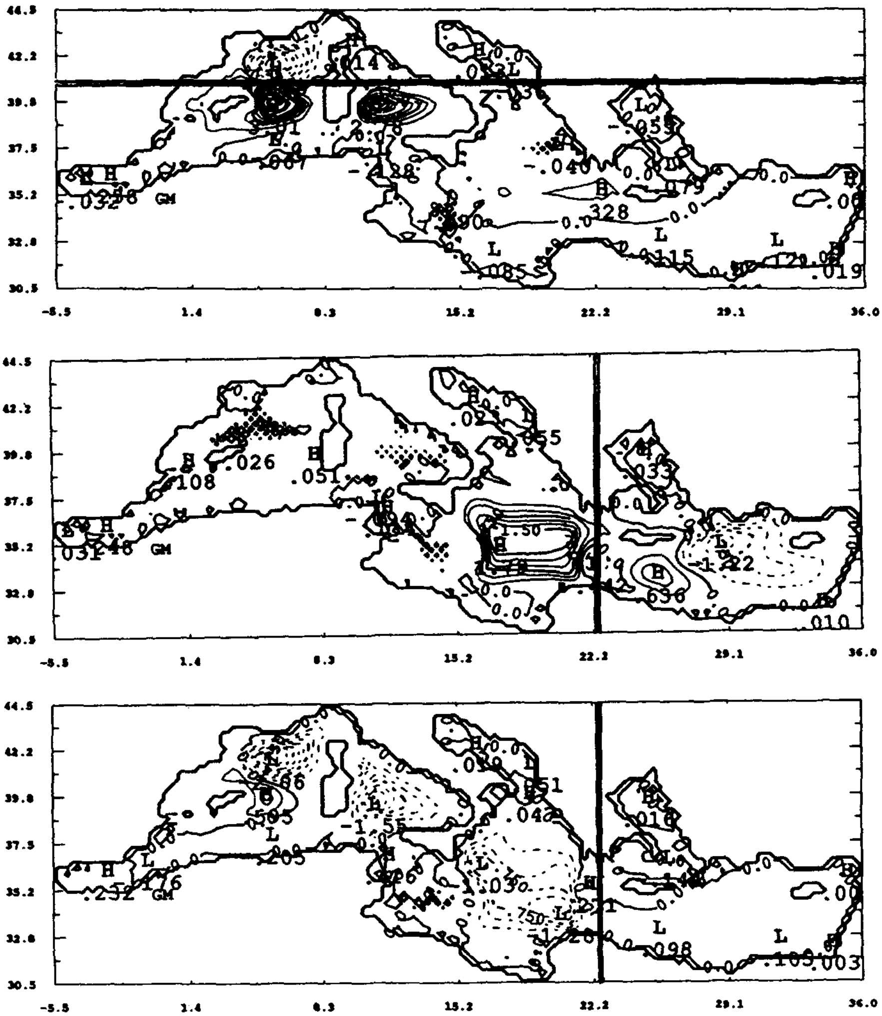

Fig. 6. Annual mean transport streamfunction for the experiments listed in Table 1 with low vertical resolution. The experiment name appears on the left hand side of the pictures. Units are in Sverdrup (10^6 m^3 s^{-1}) and the contour interval is 0.25 Sv. The dark lines cutting through the pictures indicate the location of the wind forcing terms set equal to zero (either north, east or west of the cut as explained in Table 1).

$$\zeta = \frac{m}{a^2}\left[\left(\frac{m}{H}\frac{\partial \psi}{\partial \lambda}\right)_\lambda + \left(\frac{1}{mH}\frac{\partial \psi}{\partial \theta}\right)_\theta\right]$$

is written

$$\partial_t \zeta + \vec{u}\cdot\nabla\zeta - (\zeta + f)\frac{\vec{u}\,\nabla H}{H} + \beta\frac{m}{aH}\frac{\partial \psi}{\partial \lambda} = \hat{k}\cdot\nabla\times\left(\frac{\vec{\tau}}{H}\right) + A_h\nabla^2\zeta + BT + O\left(\frac{\nabla^2 H}{H}\right) \tag{16}$$

where $f = 2\Omega \sin\theta$, $\beta = 1/a\, \partial f/\partial\theta\, 2\Omega \cos\theta/a$. BT are the baroclinic terms forcing the total transport equation, the $O(\nabla^2 H/H)$ terms are neglected and all the other symbols have been described previously. All factors H can be considered constant for the low vertical resolution case we are discussing. The BT terms are written

$$BT = \nabla\cdot\frac{1}{a}\frac{\partial}{\partial\theta}(\overline{\vec{u}\hat{u}}) - \nabla\cdot\frac{m}{a}\frac{\partial}{\partial\lambda}(\overline{\vec{u}\hat{u}}) + \frac{1}{H}J(\hat{p}(-H),H) \tag{17}$$

where $\hat{p}(-H) = \int^0_{-H} g\rho \mathrm{d}z$ and $J(\phi,\cdot) = m/a^2\,[\partial\phi/\partial\lambda\, \partial/\partial\theta - \partial\phi/\partial\theta\, \partial/\partial\lambda]$. The third term in the right hand side of (17), called Jebar term (HOLLAND, 1973; HUTHNANCE, 1984), is important only when both density and topography are present. In our case this term is clearly unimportant in most of the domain. The first and second terms in the right hand side of Eqn. (17) are also negligible in our case since the mean transport streamfunctions of experiment C1 and C5 (not shown here) are comparable. Therefore we neglect the overall BT term in the transport equation.

We divide now the streamfunction $\psi(x,y,t)$ in an annual mean or steady state part $\overline{\psi(x,y)}^t$ and an unsteady component $\psi'(x,y,t)$. The equation for the steady state vertically integrated vorticity, assuming the BT and the topographic terms to be unimportant in Eqn. (16), is

$$\overline{\vec{u}}^t\cdot\nabla\overline{\xi}^t + \beta\frac{m}{aH}\overline{\psi}^t_\lambda + \overline{\vec{u}'\cdot\nabla\zeta'}^t = \overline{\frac{1}{H}\hat{k}\times\nabla\vec{\tau}}^t + A_h\nabla^2\overline{\xi}^t. \tag{18}$$

In this equation all the terms are self explicit. We will call the first term on the left hand side the mean flow self-advection term and the third term on the left hand side the transient eddy non-linear term.

First of all, comparing experiments C2 and C1 in Fig. 6 it is evident that the annual mean barotropic circulation is given by a linear response to winds. This means that the transient eddy non-linear term in the time mean vorticity equation (18) is negligible everywhere. This is also confirmed by the low amplitude field of experiment C3 shown in Fig. 6.

The activity centers identified in the curl distribution and discussed previously are indicated again in Fig. 6. If a Sverdrup balance holds in the basin [a balance between the β term and the curl in equation (18)] the induced circulation in ψ would have the opposite sign of the curl centers. We remove the sign uncertainty in the Sverdrup balance by considering the flow to be parallel to the wind stress direction, which corresponds to a friction boundary layer that balances the wind source of vorticity (STOMMEL, 1965). Thus we can consider our gyres as Sverdrup balance gyres that are, however, generally shifted to the west with respect to the curl centers. This effect can be due to the viscous effects and the term of self-advection of vorticity in equation (18). Thus the fundamental balance in the basin is given by

$$\vec{\bar{u}}^{t} \cdot \nabla \bar{\zeta}^{t} + \beta \frac{m}{aH} \bar{\psi}^{t}_{\lambda} \simeq \frac{1}{H} \overline{\hat{k} \times \nabla \vec{\tau}}^{t} + A_h \nabla^2 \bar{\zeta}^{t} \qquad (19)$$

The importance of the β term in equation (19) is shown by experiment C4 (f constant) in Fig. 6. The dipolar structure present now in the Liguro-Provençal region has a much stronger anticyclone than in C1. In this region the β effect rotates the zonally oriented dipolar vorticity centers in the curl of Fig. 3(e) (centers I–W and II–W) in a meridionally oriented dipole with the anticyclone to the south (as it is always the case in the northern hemisphere). The anticyclone circulation is, however, almost totally dissipated in the viscous boundary layer associated with the continental borders and the Majorca–Minorca islands. In the Tyrrhenian basin the balance also seems to be dominated by equation (19), and this time viscosity and self-advection shift the circulation of Fig. 6 to the east of the curl center III–W. It is clear by comparing C1 and C4 experiments (Fig. 6) that β induces also a small western boundary intensification in the Tyrrhenian.

The EM annual mean response shows the importance of the β terms in weakening the strength of the anticyclones (IV–E and II–E in Fig. 6) and cyclones (northwest of IV–E). It is important to notice that experiment C4 needed higher dissipation than all the other experiments to level off the integrated kinetic energy of the basin. Even so the steady state circulation is stronger than in the C1 case, probably because of energy dissipation via a short wavelength Rossby wave radiation field.

The effect of the mean flow self-advection term in equation (18) can be investigated further by performing experiments with the wind forcing set to zero in different portions of the basin. This term is responsible for the self generation of the mean flow given a remote wind input of vorticity. The remote forcing response of a basin is thus connected to the following balance in equation (18).

$$J(\bar{\psi}^{t}, \bar{\zeta}^{t} + f) \simeq A_h \nabla^4 \bar{\psi}^{t}. \qquad (20)$$

In experiment S1 the wind forcing has been eliminated south of the latitude corresponding to the northern side of the Majorca island. This corresponds to force the southern Balearic basin with a net anticyclonic vorticity input from the Northern regions. As a result of this, the anticyclonic gyre in experiment S1 is stronger than the corresponding gyre of experiment C1 due to the non-linear balance of equation (20). Thus the local southern Balearic wind forcing contributes to weaken the Majorca anticyclone, which is essentially due to the curl center I–W in the northern Balearic basin.

The remaining experiments of Fig. 6 show the relative contribution of local and remote facing to the mean circulation in the Ionian basin. In experiment S2 the winds have been artificially set equal to zero west of the western tip of the Peloponnesus. In Fig. 6, the experiment S2 results show that the anticyclonic streamfunction center in the Ionian is remotely forced by the wind stress in the eastern part of the EM basin. Thus the non-linear balance in equation (20) is important in the Ionian basin. The mean response to local changes in the wind stress curl is cyclonic (experiment S3 in Fig. 6). Thus the steady state Ionian circulation is made up of two opposite contribution remotely and the other locally forced, which sum up to give the weak anticyclonic mean circulation of experiment C1 in Fig. 6.

In the high resolution experiment (H1) the mean circulation looks very similar to the C1 experiment result shown in Fig. 6. However, the Ionian anticyclonic mean circulation is further reduced in amplitude, showing that for the kind of climatological forcing considered, much of the remote response of the Ionian is eliminated with a more detailed description of the topographic effects.

(b) *The seasonal circulation*

In Fig. 7 we show the transport streamfunction every two months for one of the repeating cycles of the C1 case of Fig. 5. We examine now the seasonal variations in the WM and EM separately.

(*i*) *The WM seasonal cycle*. The WM seasonal transport variations are large with respect to the mean circulation (Fig. 6), particularly in the southern Balearic Basin and eastern Tyrrhenian Sea. A reversal of the Winter circulation occurs in the southern Balearic basin. During the autumn–winter months (November and January) the circulation is cyclonic in the whole Balearic basin. During the Spring the southern cyclonic circulation weakens and is replaced by an anticyclonic gyre, which reaches its peak amplitude during July and then it weakens again.

The Tyrrhenian has a prevalent cyclonic circulation except for the summer and autumn months when the circulation weakens considerably. The July conditions of Fig. 7 show evidence for the development of an anticyclonic circulation in the Eastern part of the Tyrrhenian basin, which expands and propagates in the middle of the basin until September. These results substantially confirm the one-layer reduced gravity general circulation model of HEBURN (1987) relative to the WM basin.

(*ii*) *The EM seasonal cycle*. In the EM the only quasi-permanent feature is the cyclonic circulation in the northern Levantine basin, which, however, weakens considerably and shifts of position during Summer. The magnitude of the seasonal transports is generally larger than the mean transports of Fig. 6 both in the Ionian and Levantine basins. In the Levantine basin the Winter circulation is formed by a cyclonic gyre which is intensified along the northern Turkish–Greek coastlines. This gyre is quasi-permanent and its position shifts around the position of the mean gyre I–E (Fig. 6). During the spring an anticyclonic circulation develops southeast of the cyclonic gyre and it amplifies while it propagates northwestward reaching a maximum amplitude in May. The location of this anticyclone is mostly on the southeast side of Crete, as shown by the steady state gyre II–E of Fig. 6.

The Ionian circulation is completely reversed between January and July conditions. The gyres are western boundary intensified. There is evidence of westward propagation of modes in the Northern Ionian basin, where the variance of the wind stress curl has a maximum [region V–E in Fig. 3(f)]. This propagation is very fast (about 2 months between January and March and September–November) and it is confined to the Northern Ionian area. PIERINI (1990) has shown that for wind forcing timescales greater than 1 month, the Mediterranean response is likely to be composed by travelling Rossby modes. Our results suggest that the wind curl annual and semi-annual harmonic components (Fig. 4) can produce this signal.

We also examined the seasonal response of experiments S2 and S3 and compared it with the control experiment, C1. The results (not shown) demonstrate that about 70% of the amplitude of the Ionian circulation is controlled by local wind changes (S3) and 30% by remote forcing from the Levantine basin (S2). The remote response signal (S2) is particularly important in the Southern Ionian basin.

The presence of westward propagation in the Levantine basin (Fig. 8), shows a time–longitude cross section in the EM basin (Hovmoller diagram). The cross section for the

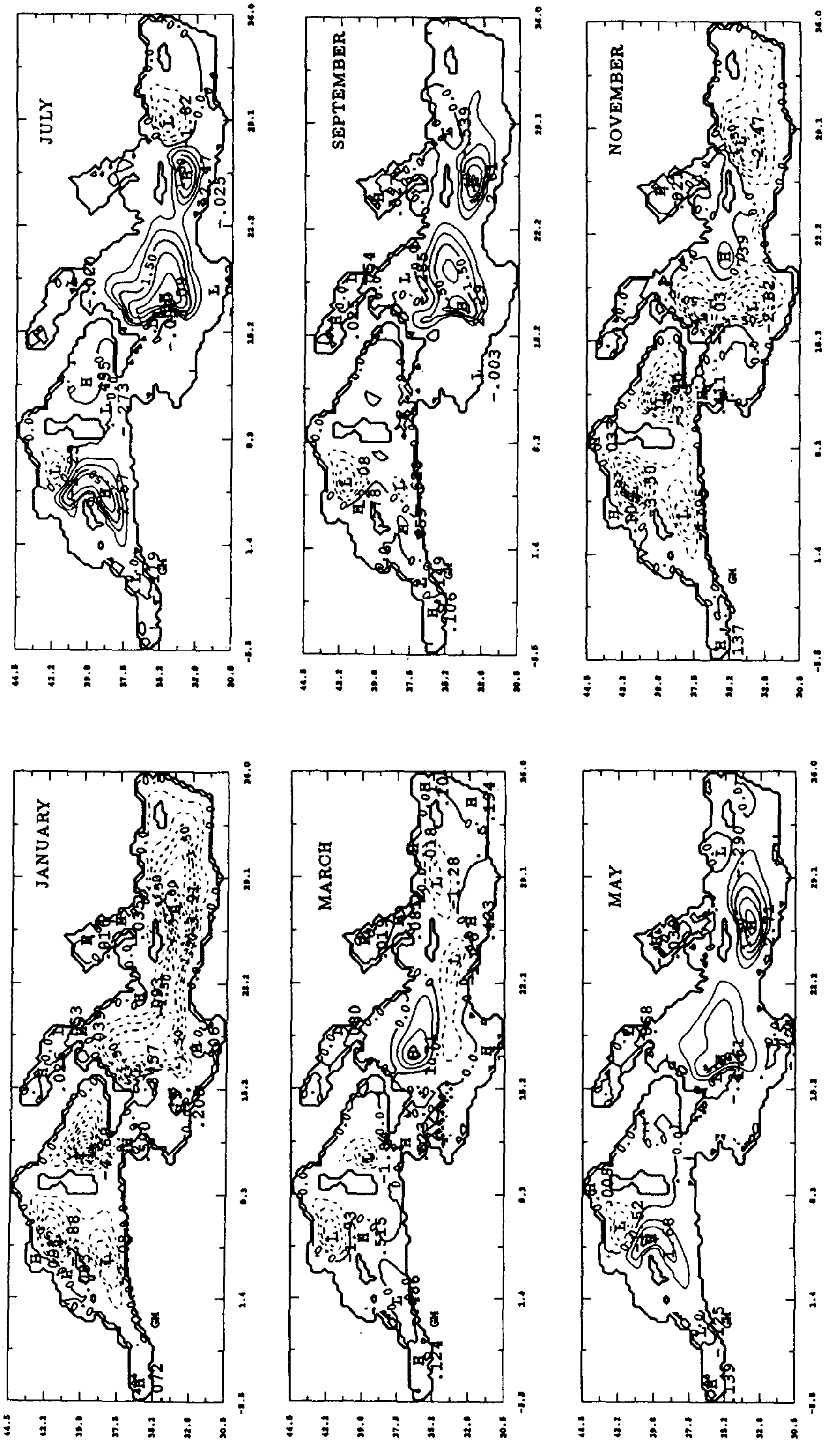

Fig. 7. Seasonal cycle in the transport streamfunction for experiment C1. The pictures are instantaneous fields taken at the end of the month indicated in the upper right corner of each plot. Units are in Sverdrup and the contour interval is 0.5 Sv.

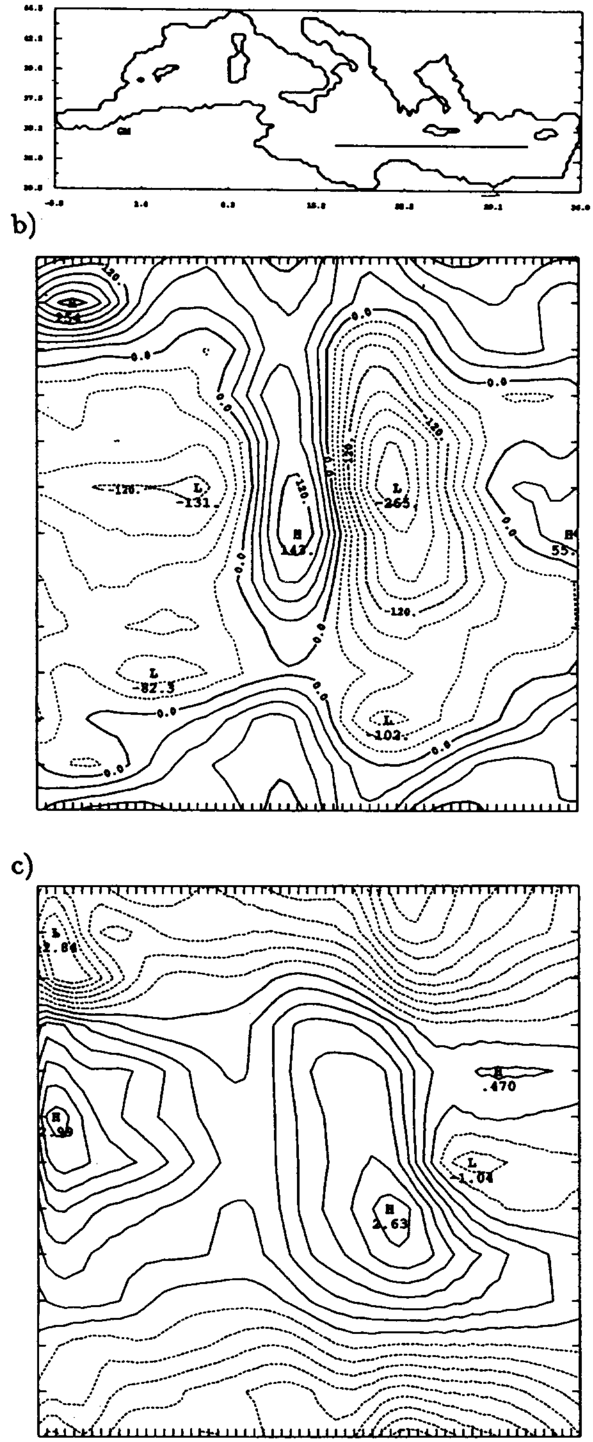

Fig. 8.

wind stress curl [Fig. 8(b)] indicates clearly the presence of a 1-year period change in the wind curl along each longitude point of the section except for the area southwest of Crete. However, neither propagation nor simple structure is evident in this wind stress curl section while some propagation is noticeable in the Hovmoller diagram of the transport streamfunction [Fig. 8(c)]. Again, WILLEBRAND *et al.* (1980) have shown that when the forcing has an horizontal scale greater than ~100 km and the period is larger than 1 month, Rossby wave propagation response can be excited.

In the Ionian basin the major transport signal is located north of the section shown in Fig. 8. In Fig. 9 an Hovmoller diagram compares the wind stress curl and the results of C1, C4 experiments along a section in the central Northern Ionian basin. In Fig 9(b) it is evident again the annual cycle in the wind stress curl. Figure 9(c) shows the local and non propagating response of the Ionian basin to this forcing. Figure 9(d) shows the westward propagation and intensification of the circulation pattern induced by the annual component of the wind stress curl. To gain confidence in these results we performed experiment H1, which has higher vertical resolution. The new vertical levels were chosen to further improve the numerical resolution of the upper thermocline level, and we also obtained some improvement of the description of the topography. This case was designed as another kind of sensitivity experiment to determine the reliability of the previous results.

The seasonal cycle for experiment H1 is shown in Fig. 10. In the WM the gyres are similar in shape to the C1 case, but some of them are substantially reduced in amplitude, presumably because of topographic effects. This reduction is consistent with similar results obtained for the North Atlantic basin by HOLLAND (1973), who showed that a substantial reduction in the transport is observed if a more detailed description of the topography is included in the model. It is interesting to note that the seasonal variability of the gyres is still present and it seems to have the same dynamical characteristics revealed in the lower vertical resolution case.

A similar weakening of the transport compared to the C1 case is present in the EM. Overall, similar features as in the low resolution case appear. The number of gyres, their seasonal variability and propagation are consistent with the low resolution case, with the exception of the cyclonic feature south of Crete which is better defined in the H1 experiment. Substantial differences appear in the Ionian basin. The bottom topography modulates the shape of the gyre so that its geographical distribution is different from C1. However, the seasonal cycle can still be detected with much the same characteristics as in C1. The speed of transition from the winter to summer circulation pattern is somewhat different, but the amplitude extrema of the Ionian gyres is researched in the same months.

Fig. 8. Hovmoller diagram for transport streamfunction and wind stress curl in the EM. The time on the ordinate axis goes from one January to the next included and with a time interval of 1 month (13 ticks). The ticks on the abscissa indicate the grid points of the cross section from west to east. (a) Longitudinal cross section location at 34°N. (b) Wind stress curl time-longitude contour plot. The annual mean wind-stress curl has been subtracted. Units are in 10^{-10} dyne cm^{-3} and the contour interval is 30 units. (c) Transport streamfunction time–longitude contour plot. Units are in 0.4 Sv.

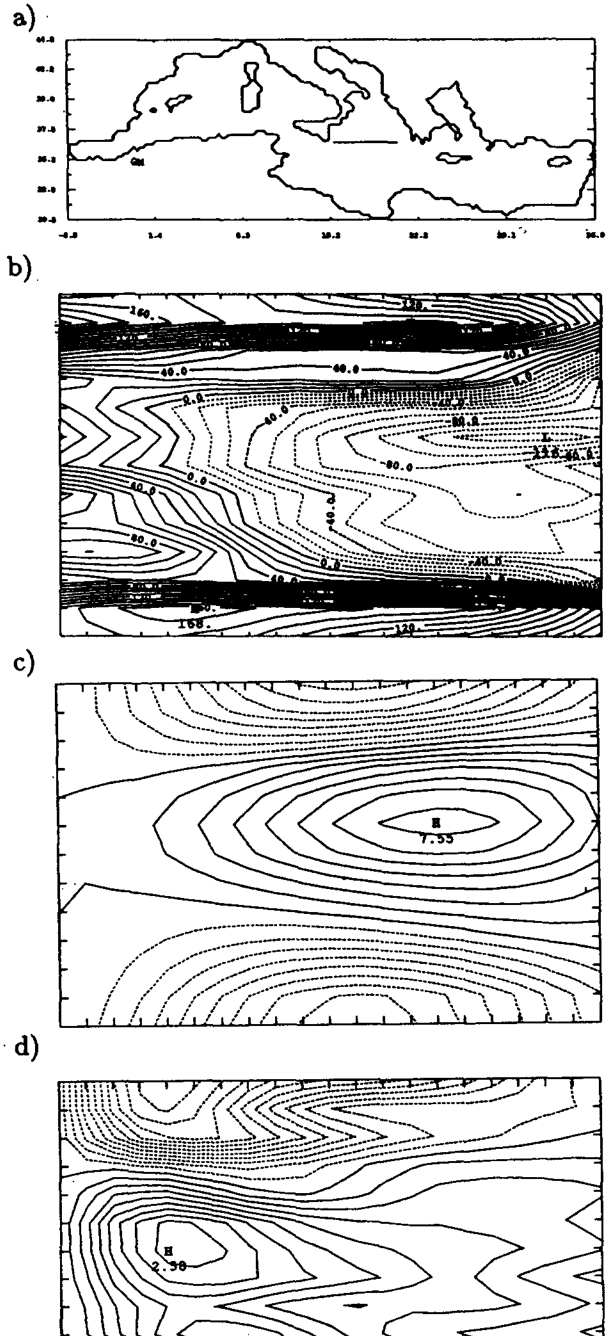

Fig. 9.

4. THE BAROCLINIC CIRCULATION

We now consider the baroclinic part of the seasonal response in experiment C1. Firstly, we show in Fig. 11 the dynamic height fields calculated from the temperature and salinity vertical profiles. The reference level is chosen to be at 1000 m.

The summer surface dynamic height (30 m) in the WM shows an Algerian Gyre with the North African Current displaced along its Northern border. The Liguro-Provençal cyclonic gyre is quite small and its center is probably displaced too far north. A cyclonic circulation dominates the Tyrrhenian basin. At 490 m the summer and winter circulation is too weak probably due to the low vertical and horizontal resolution of the model. The missing effect of Gibraltar inflow–outflow system could be partly responsible for this result. At this depth, the North African Current is westward during summer and almost absent during winter. The flow is generally northward in the central Balearic basin during summer and the Liguro-Provençal gyre and Tyrrhenian gyres are intensified during winter.

In the EM and at the surface, the Levantine basin circulation is composed by a single gyre center, that might correspond to the Rhodes gyre, which weakens in strength and reduces in size during summer. In the southern part of the Levantine basin and during the summer, the circulation shows a weak anticyclonic gyre located at the southern border of the Rhodes gyre which disappears during winter, replaced by a strong EM North African Current. In the Ionian basin the model shows the shift between summer and winter of the EM North African Current system. This current moves from a position hugging the Lybian coasts in winter to the central part of the Ionian basin in summer. Thus the purely wind induced baroclinic motion contains a general shift of the EM North African Current in the Ionian basin and the reversal of the circulation between summer and winter in the southern part of the Ionian basin. The high resolution central experiment results are very similar to Fig. 11, confirming that the vertical resolution in this case is not crucial given the other model choices of parameters.

The baroclinic velocity fields at 30 m for 3 different months (Fig. 12) show quantitatively the current seasonal changes in magnitude and direction. The summer weakening of the EM North African Current is evident as much as its shift to the center of the Ionian basin. Furthermore, during winter a northern boundary intensified jet forms along the Turkish coasts. This jet, the Asia Minor Current (Robinson *et al.*, 1991) undergoes a seasonal weakening during spring and summer.

Finally we show the temperature and salinity vertical structure in the model. The levels below the surface are left free to evolve by the models equations (4) and (5), and it is interesting to look to the effect of wind induced advection on the changes in temperature and salinity. In Fig. 13(a) we show the temperature and salinity sections for the initial time, e.g. the interpolated Levitus (1983) data to the model grid points. Figure 13(b) and (c) show that the model makes a sharper thermocline at about 100 m as seen in hydrological

---

Fig. 9. Hovmoller diagram for transport streamfunction in the Ionian basin. The time on the ordinate axis goes from one January to the next included and with a time interval of 1 month (13 ticks). The ticks on the abscissa indicate the grid points of the cross section from west to east. (a) Longitudinal cross section location at 36.5°N. (b) Wind stress curl along the section. Units are in 10^{-10} dyne cm^{-3} and the contour interval is 10 units. (c) Transport streamfunction for C4 in units of Sverdrup. The contour interval is 1 unit. (d) Transport streamfunction for C1 in units of Sverdrups. The contour interval is 0.3 units.

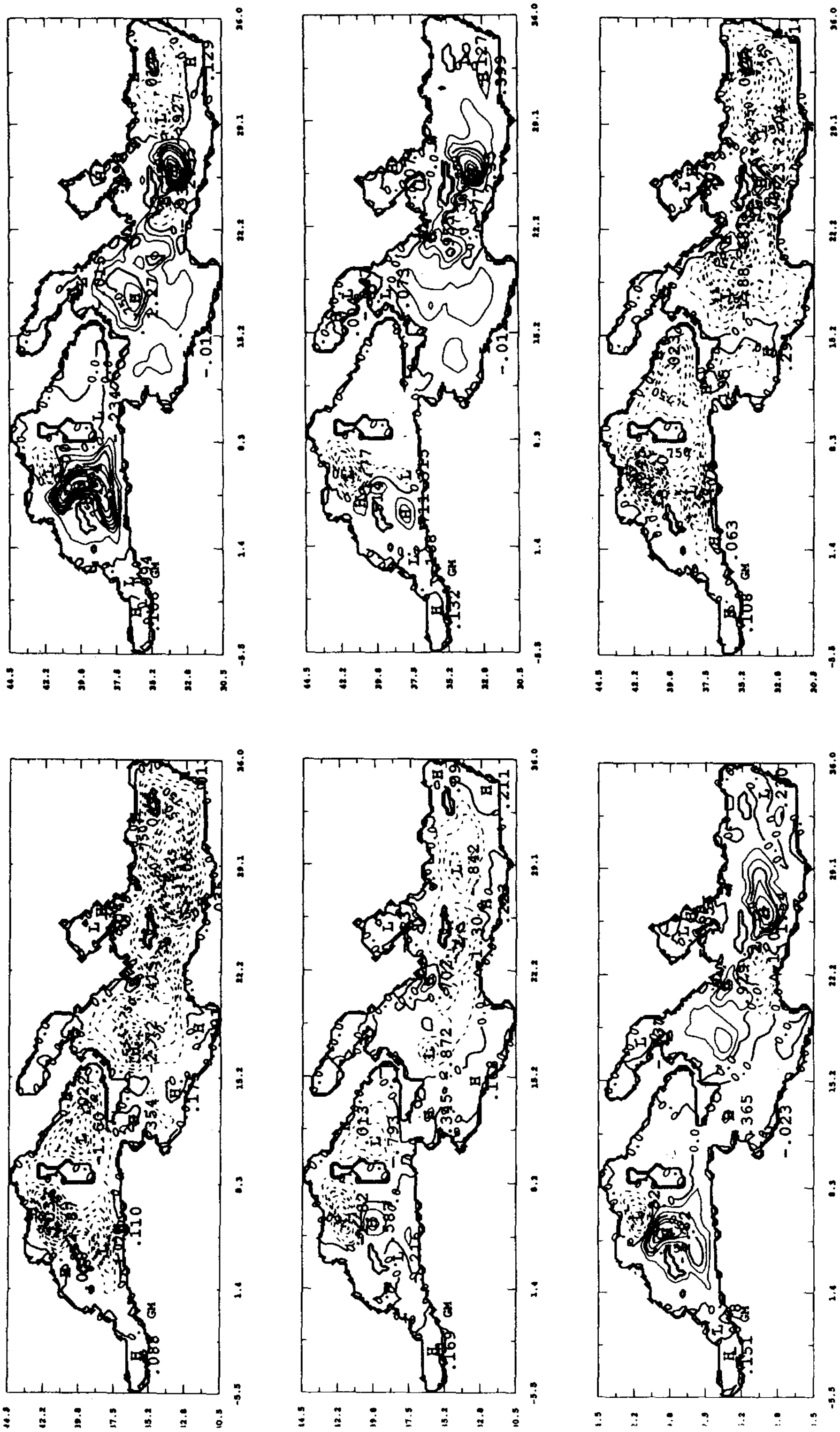

Fig. 10. Seasonal cycle in the transport streamfunction for experiment H1. The pictures are instantaneous fields taken at the end of the month indicated in the upper right corner of each plot. Units are in Sverdrup and the contour interval is 0.25 Sv.

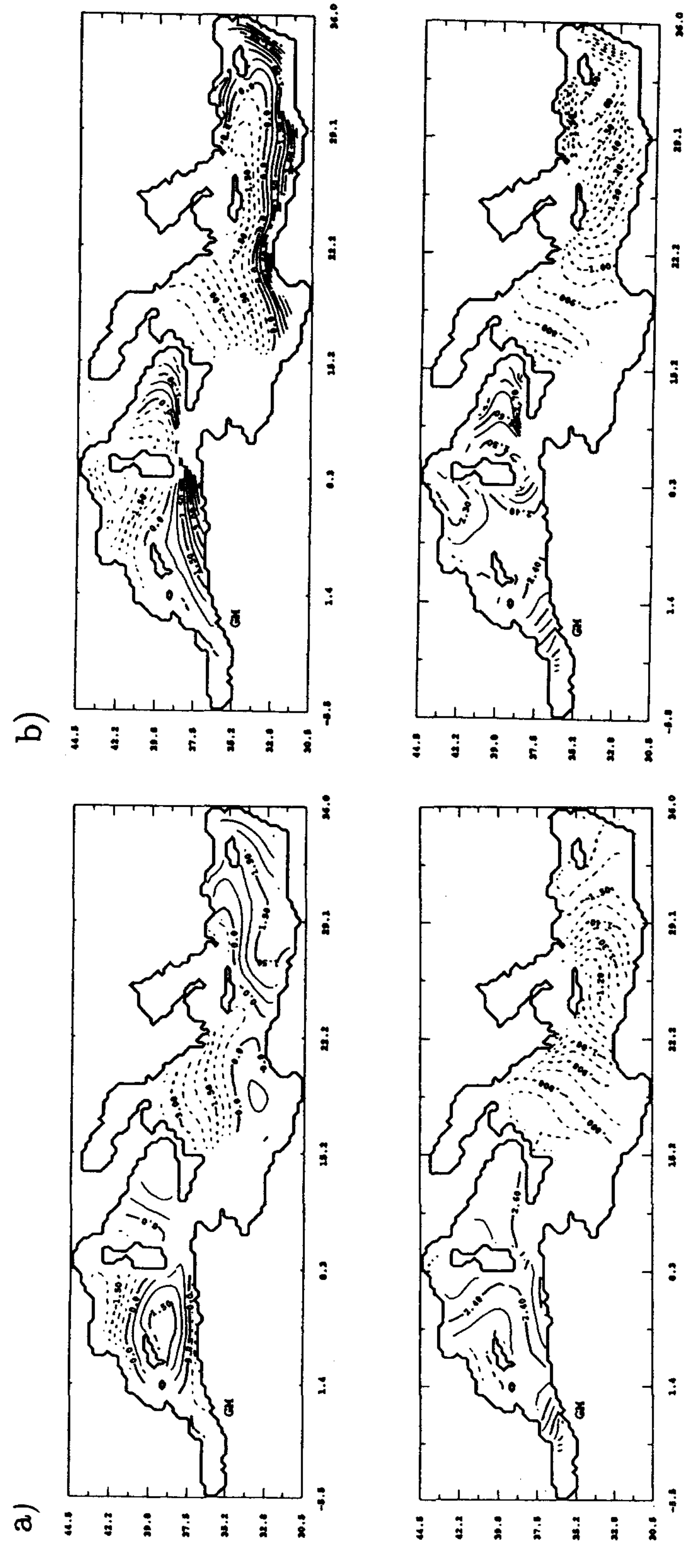

Fig. 11. Dynamic height fields referred to 1000 m. (a) July conditions for the first model level (top left) at 30 m and the level at 490 m (bottom left). (b) January conditions for the model level at 30 m (top right) and at 490 m (bottom right). Units are cm and we show the deviations from the horizontal averages (-60 cm at 30 m and -36 cm at 490 m.)

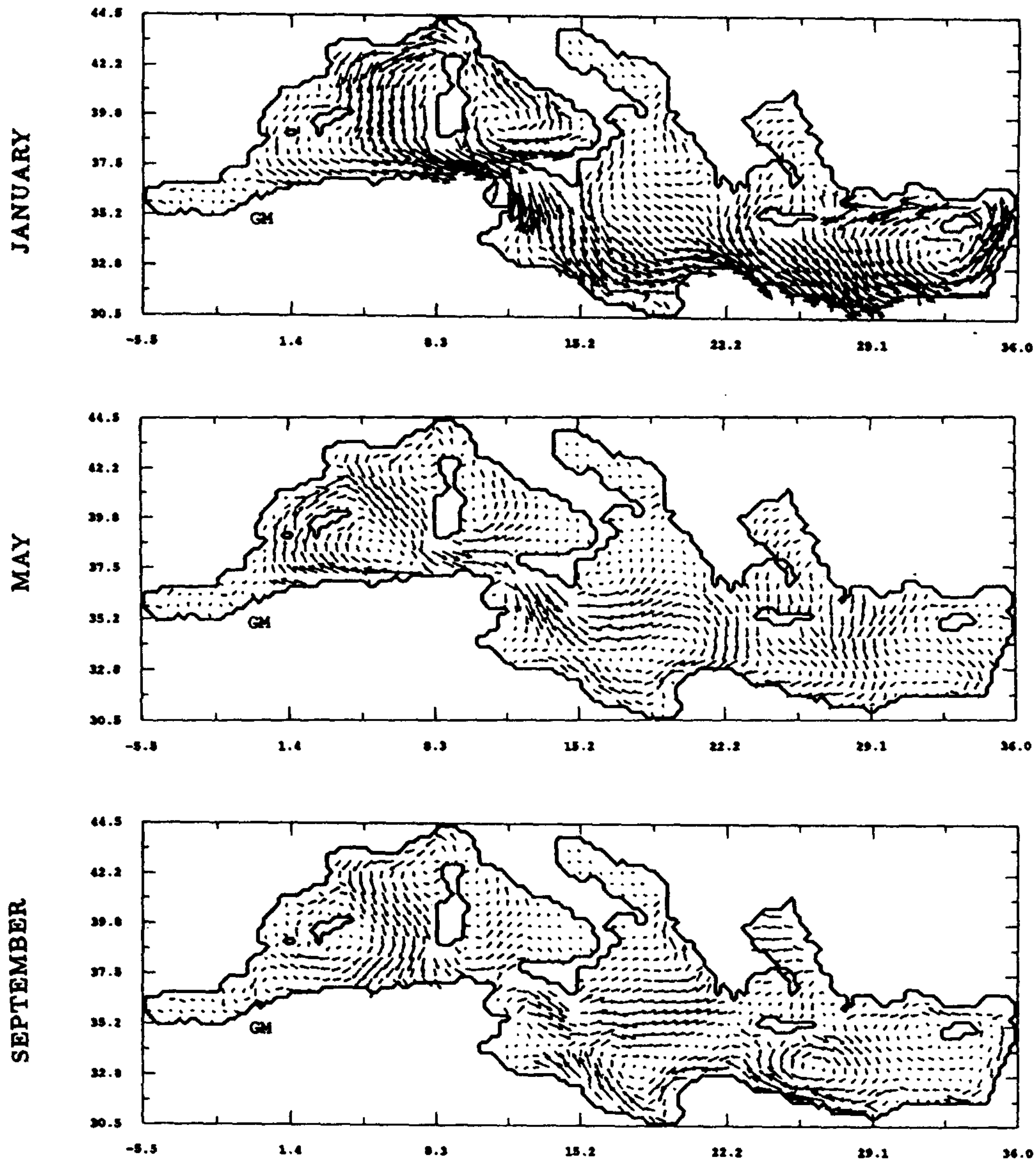

Fig. 12. Total model velocities at the model level 1 (30 m) for January, May and September. The maximum velocities of about 5 cm s^{-1} are reached during January.

data for the EM (HECHT *et al.*, 1989). Furthermore Levantine Intermediate Water (LIW) main body (indicated by the sub-surface salinity maximum) starts to be displaced more in the southern part of the Ionian basin than in the initial condition. In addition the core of LIW in the model simulations is limited between 200 and 600 m only. It is also evident that the slope of the isotherms is changing from anticyclonic to cyclonic between September and January respectively. This is the temperature signature of the velocity field reversal in the Ionian due to local winds and the induced Rossby wave motion.

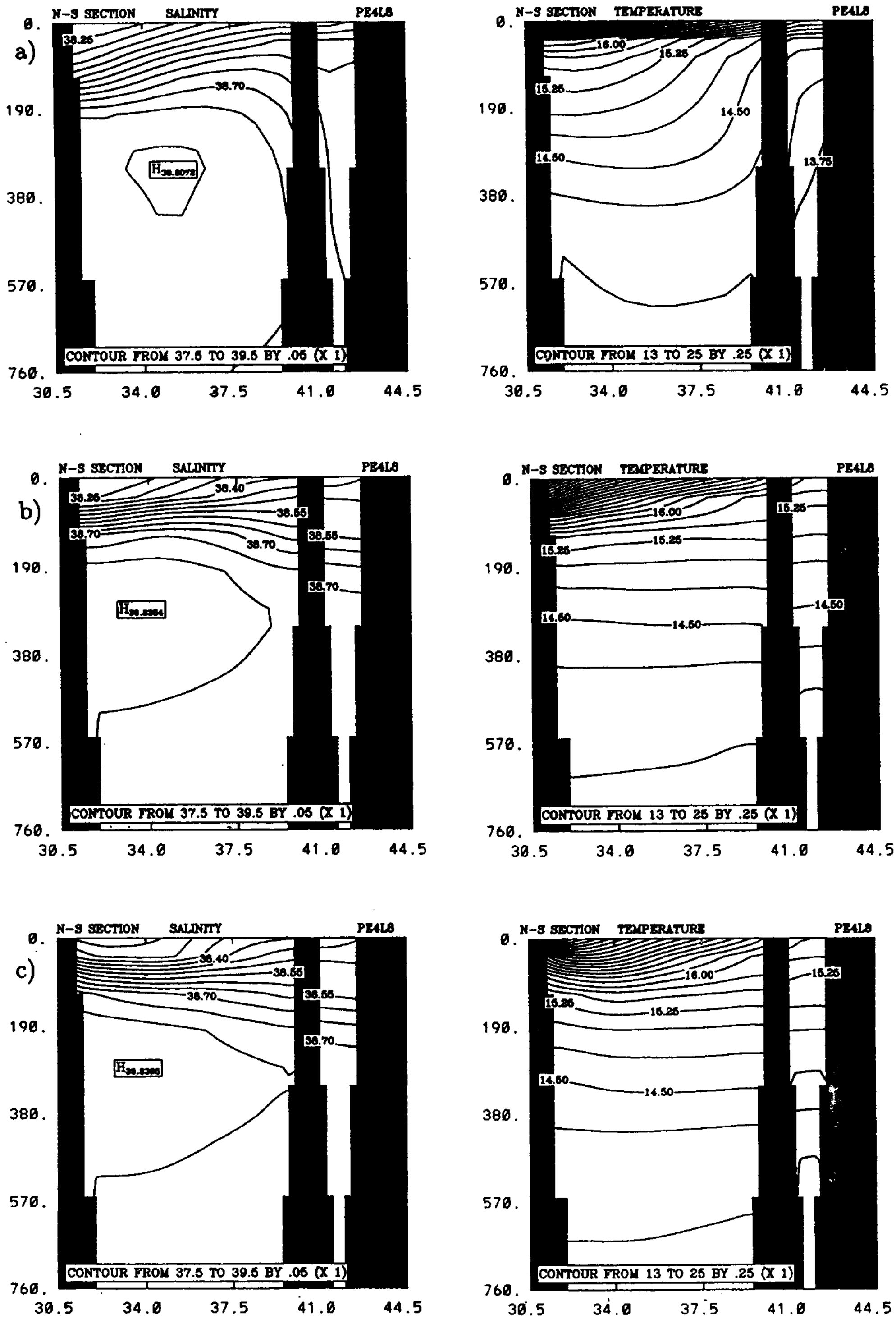

Fig. 13. Temperature (left column) and salinity (right column) north–south section at 17.75°E. (a) initial condition, (b) January conditions, (c) September conditions.

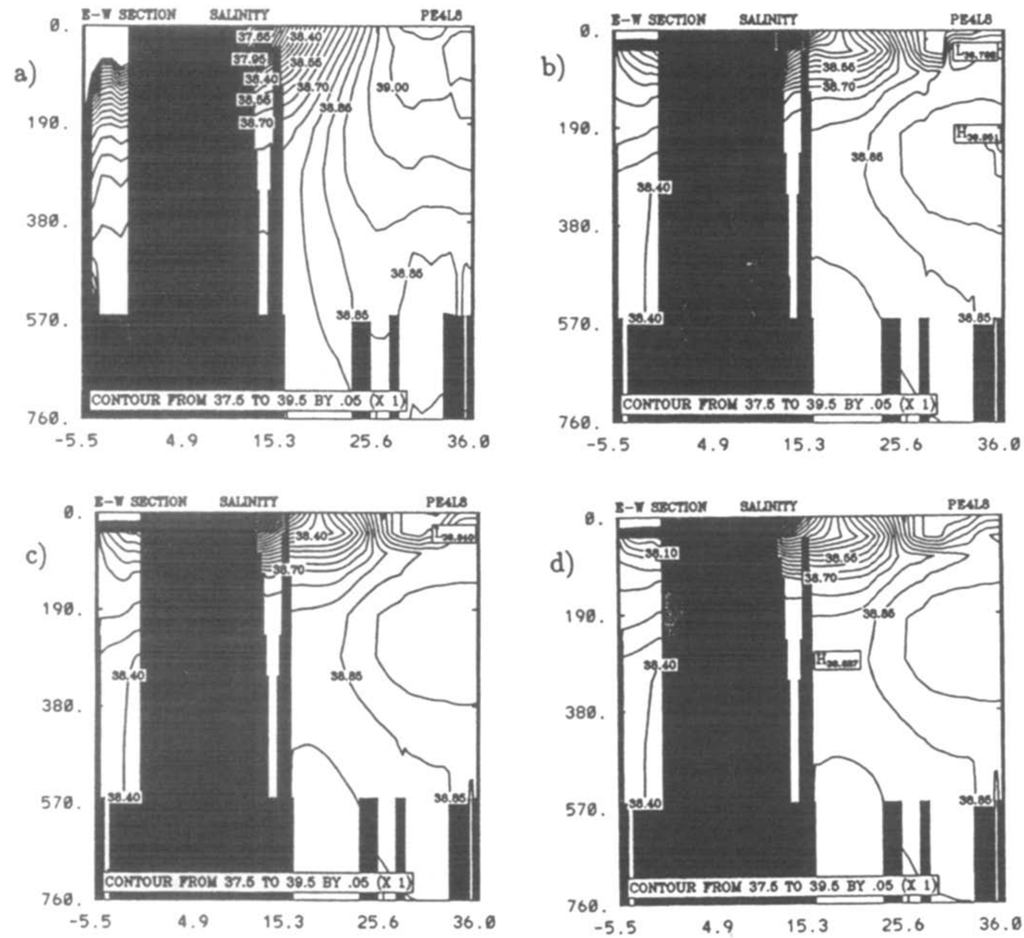

Fig. 14. Salinity west–east sections at 35.75°N. (a) Initial condition, (b) January, (c) May and (d) September conditions.

Another important feature of Mediterranean water masses is the subsurface Atlantic water salinity minimum (HECHT *et al.*, 1989). In the initial condition [Fig. 14(a)] salinity structure in an east–west cross-section at 35.75°N of the basin, no subsurface minimum in salinity is evident, only a gradual increase of salinity toward the east is present. In the model simulation the subsurface minimum is formed [Fig. 14(b)–(d)] and it extends further to the east during the summer months (Fig. 14d). Here also we see the tendency by the model to form a well-defined body of LIW extending from the easternmost coast of the model to the longitude of about 25°E.

5. SUMMARY AND CONCLUSIONS

The barotropic transport in the overall Mediterranean basin is defined by sub-basin scale gyres that are either persistent (like the Liguro-Provençal gyre) or totally seasonal (like in the Ionian basin). The annual average circulations is given by a Sverdrup balance modified by viscosity. The seasonal circulation shows generally weaker currents in summer than in winter and the reversal of currents in major subportions of the basin.

The annual period harmonic component of the wind stress field is responsible for the largest wind stress curl changes, which in turn excite a sudden oceanic response composed by Rossby modes and westward intensification. The β-effect is shown to be important for the realistic positioning of the Liguro-Provençal Gyre and for shaping the response to seasonal changes in winds. As PIERINI (1990) has shown in a study of an idealized Mediterranean basin, at these forcing frequencies Rossby waves are likely to be excited by the action of the wind stress curl changes.

The model results show that the wind-induced motion can contribute substantially to the shift of the North African Current from its winter position along the North African coasts to the center of the Balearic and Ionian basin in summer.

The advection of temperature and salinity by the wind induced motion and the related convective adjustment mixing is able to form a well defined LIW subsurface pool and a sub-surface salinity minimum usually associated with water masses of Atlantic origins.

The present model is a first approximation to the wind driven general circulation problem of the Mediterranean basin. The realistic topography and time-dependent heat and salt fluxes at the air–sea interface are necessary additions to the present model formulation. Realistic parameterizations of the vertical mixing processes, of the surface energy balance and of the Gibraltar inflow–outflow are important components that need to be included in the model. However, we have shown that new and interesting phenomena are involved in the wind adjustment processes in a limited extension basin like the Mediterranean Sea. Thus, even a simple model like the one presented here exhibit a rich and complex spectrum of physical phenomena that can lead to the description of some dynamical mechanism that can be relevant to the wind driven Mediterranean Sea general circulation.

Acknowledgements—This paper would have never been written without the enthusiastic support of Mike Cox that provided us with the original model code. Mike was always eager to be informed on our effort and it was his open attitude that made it possible. We thank Dr Simona Masina for helping us with some calculations. This work was partially supported by the European Communities under the contract MAST-0039-C and by a grant of the Progetto Strategico "Oceanografia e Tecnologie marine". The calculations were carried out at CINECA, Bologna, Italy on a CRAY X-MP and Y-MP computer. We thank Sanzio Bassini from CINECA for invaluable assistance.

REFERENCES

BRYAN K. (1969) A numerical model for the study of the world ocean. *Journal of Computational Physics*, **4**, 347–376.

COX M. D. (1984) *A primitive equation three-dimensional model of the ocean*. GFDL Ocean Group Technical Report No. 1, GFDL/NOAA, Princeton University.

COX M. D. (1987) An eddy resolving numerical model of the ventilated thermocline: Time dependence. *Journal of Physical Oceanography*, **17**, 1044–1056.

CREPON M., M. BOUKTHIR, B. BARNIER and F. AIKMAN III (1989) Horizontal ocean circulation forced by deep water formation. Part I: an analytical study. *Journal of Physical Oceanography*, **19**, 1781–1792.

HEBURN G. W. (1987) The dynamics of the western Mediterranean Sea: a wind forced cast study. *Annales Geophysicae*, **5B**(1), 61–74.

HECHT A., N. PINARDI and A. R. ROBINSON (1988) Currents, Water masses, eddies and jets in the Mediterranean Levantine basin. *Journal of Physical Oceanography*, **18**(10), 1320–1353.

HELLERMAN S. and M. ROSENSTEIN (1983) Normal wind stress over the world ocean with error estimates. *Journal of Physical Oceanography*, **13**, 1093–1104.

HOLLAND W. R. (1973) Baroclinic and topographic influences on the transport in western boundary currents. *Geophysics of Fluid Dynamics*, **4**, 187–210.

HUTHNANCE J. M. (1984) Slope currents and "JEBAR". *Journal of Physical Oceanography*, **14**, 795–810.

LEVITUS S. (1982) *Climatological Atlas of the World Oceans*. NOAA Professional Paper No. 13. U.S. Government Printing Office. Washington, D.C.

MALANOTTE-RIZZOLI P. and A. BERGAMASCO (1989) The circulation of the Eastern Mediterranean. Part I. *Oceanologica Acta*, **12**(4), 335–351.

MALANOTTE-RIZZOLI P. and A. BERGAMASCO (1991) The wind and thermally driven circulation of the eastern Mediterranean Sea. Part II: the baroclinic case. *Dynamics of Atmospheres and Oceans*, **15**, 355–371.

MENZIN A.B. and L. V. MOSKALENKO (1982) Calculation of Wind-driven currents in the Mediterranean Sea by the Electrical simulation method (Homogeneous Model). *Oceanology*, **22**(5), 537–540.

MILLIFF R. F. and A. R. ROBINSON (1991) Structure and dynamics of the Rhodes gyre system and dynamical interpolation for estimates of the mesoscale variability. *Journal of Physical Oceanography*, **22**, 317–337.

OVCHINNIKOV I. M. and FEDOSEYEY (1965) The horizontal circulation of the water of the Mediterranean Sea during the summer and winter seasons. 185–201.

OZSÖY E., A. HECHT and AND Ü.ÜNLÜATA (1989) Circulation and hydrography of the Levantine basin: results of POEM coordinated experiments 1985–1986. *Progress in Oceanography*, **22**, 125–170.

PIERINI S. (1990) A divergent quasigeostrophic model for wind driven oceanic fluctuations in a closed basin. *Dynamics of Atmospheres and Oceans*, **14**, 259–277.

STANEV E. V., H. J. FRIEDRICH and S. V. BOTEV (1989) On the seasonal response of intermediate and deep water to surface forcing in the Mediterranean Sea. *Oceanologica Acta*, **12**(2), 141–149.

STOMMEL H. (1965) *The Gulf Stream: a physical and dynamical description*. University of California Press, Berkeley, 248 pp.

WILLEBRAND J., S. H. G. PHILANDER and R. C. PACANOWSKI (1980) The oceanic response to large-scale atmospheric disturbances. *Journal of Physical Oceanography*, **10**, 411–429.